Lansoprazole Inhibits the Development of Sessile Serrated Lesions by Inducing G1 Arrest via Skp2/p27 Signaling Pathway

Tomoyuki Kawaguchi,[1] Koichi Okamoto,[1] Shota Fujimoto,[1] Masahiro Bando,[1] Hironori Wada,[1] Hiroshi Miyamoto,[1] Yasushi Sato,[2] Naoki Muguruma,[1] Katsuhisa Horimoto,[3,4] Tetsuji Takayama[1]

[1]Department of Gastroenterology and Oncology, Institute of Biomedical Sciences, Tokushima University Graduate School, 3-18-15 Kuramoto-cho, Tokushima 770-8503, Japan

[2]Department of Community Medicine for Gastroenterology and Oncology, Tokushima University Graduate School of Biomedical Sciences, 3-18-15 Kuramoto-cho, Tokushima 770-8503, Japan

[3]Molecular Profiling Research Center for Drug Discovery (molprof) National Institute of Advanced Industrial Science and Technology (AIST), 2-3-26 Aomi, Koto-ku, Tokyo 135-0064, Japan

[4]SOCIUM Inc, 2-4-7 Aomi, Koto-ku, Tokyo 135-0064, Japan

Short title: Chemoprevention targeting SSL

Correspondence to: Tetsuji Takayama, M.D., Ph.D., Department of Gastroenterology and Oncology, Institute of Biomedical Sciences, Tokushima University Graduate School, 3-18-15, Kuramoto-cho, Tokushima, 770-8503, Japan.

Tel: +81-88-633-7122

Fax: +81-88-633-9235

E-mail: takayama@tokushima-u.ac.jp

Word count of the manuscript: 5973 words

Abstract

Background: Although the serrated-neoplasia pathway reportedly accounts for 15%-30% of colorectal cancer (CRC), no studies on chemoprevention of sessile serrated lesions (SSLs) have been reported. We searched for effective compounds comprehensively from a large series of compounds by employing Connectivity Map (CMAP) analysis of SSL-specific gene expression profiles coupled with in vitro screening using SSL patient-derived organoids (PDOs), and validated their efficacy using a xenograft mouse model of SSL.

Methods: We generated SSL-specific gene signatures based on DNA microarray data, and applied them to CMAP analysis with 1309 FDA-approved compounds to select candidate compounds. We evaluated their inhibitory effects on SSL-PDOs using a cell viability assay. SSL-PDOs were orthotopically transplanted into NOG mice for in vivo evaluation. The signal transduction pathway was evaluated by gene expression profile and protein expression analysis.

Results: We identified 221 compounds by employing CMAP analysis of SSL-specific signatures, which should cancel the gene signatures, and narrowed them down to 17 compounds. Cell viability assay using SSL-PDOs identified lansoprazole as having the lowest IC50 value (47 μM) among 17 compounds. When SSL-PDO was orthotopically transplanted into murine intestinal tract, the tumor grew gradually. Administration of lansoprazole to mice inhibited the growth of SSL xenograft whereas the tumor in control mice treated with vehicle alone grew gradually over time. The Ki67 index in xenograft lesions from the lansoprazole group was significantly lower compared with the control group. Cell cycle analysis of SSL-PDOs treated with lansoprazole exhibited a significant increase in G1 phase cell population. Microarray and protein analysis revealed that lansoprazole downregulated Skp2 expression and upregulated p27 expression in SSL-PDOs.

Conclusions: Our data strongly suggest that lansoprazole is the most effective chemopreventive agent against SSL, and that lansoprazole induces G1 cell cycle arrest by downregulating Skp2 and upregulating p27 in SSL cells.

Keywords: sessile serrated lesion, chemoprevention, connectivity map, organoid, lansoprazole

Introduction

Colorectal cancer (CRC) is one of the leading causes of cancer-related mortality worldwide [1]. CRC develops mainly from adenomatous polyps as precursor lesions (adenoma-carcinoma sequence), whereas the serrated neoplasm pathway, in which serrated polyps give rise to cancer, has been identified in the last 2 decades as an alternative pathway [2-6]. The serrated-neoplasia pathway is reported to account for approximately 15% to 30% of CRCs [4, 7]. Serrated colorectal lesions are largely classified into 3 categories: hyperplastic polyp (HP), sessile serrated lesion (SSL), and traditional serrated adenoma (TSA) [8]. SSLs, previously referred to as sessile serrated adenomas/polyps, are considered precursor lesions of the CRC that has molecular features of CpG island methylator phenotype (CIMP), actionable BRAF mutations (V600E), and high microsatellite instability (MSI-H) [9-12]. Because the majority of this cancer subtype derive from the serrated-neoplasia pathway and shows a very poor prognosis [13-15], the development of agents effective for the chemoprevention of SSLs is an important strategy.

No prospective chemopreventive study targeting SSLs has been reported to date. Wallace et al. evaluated chemopreventive effects against serrated polyps retrospectively using pooled data from previous randomized clinical trials for colorectal adenoma. They suggested that aspirin may reduce the risk of serrated polyps in the right-side colon [16]. However, all 3 kinds of serrated polyps (SSL, HP and TSA) were categorized as a single lesion type because the concept of serrated polyps was first proposed by Jass et al. in 2002 [17] and the pathological classification of serrated polyps was not defined when these randomized controlled trials were performed (1994-2003). Thus, a chemopreventive strategy for the SSL-cancer sequence has not yet been well established.

It is important for the development of chemopreventive agents to extensively survey numerous compounds/drugs based on omics data obtained from targeted precancerous

lesions. The Connectivity Map (CMAP) is a database of gene expression profiles from human cell lines treated with 1309 different compounds (e.g., Food and Drug Administration [FDA]-approved drugs), which can be used to score the ability of each compound/drug to counteract disease-specific signatures obtained by DNA microarray analysis of the disease [18]. A number of studies have been reported using CMAP analysis for common diseases such as diabetes and various cancers such as breast and prostate cancer, some of which are expected to be leveraged in clinical practice [19-21]. Therefore, the application of CMAP analysis to SSL makes it possible to identify effective candidate compounds comprehensively from a vast library of FDA-approved compounds.

Until recently, it has been difficult to culture SSL cells in vitro for an extended period of time. Therefore, few studies on SSL using SSL cell culture in vitro have been reported. Moreover, no animal model of SSL has been established. Thus, in vitro experiments to evaluate the preventive effect of compounds/drugs against SSL have not yet been documented to date. Sato et al. reported an intestinal organoid culture technique that enables in vitro long-term 3D culture of intestinal cells, such as normal colonic mucosa and colonic polyps, using endoscopic biopsies or surgically resected tissue [22]. Sugimoto et al. reported orthotopic xenotransplantation of human intestinal organoids into immunosuppressed mice [23]. Therefore, using this organoid culture and its orthotopic xenotransplantation techniques, we can evaluate inhibitory effects of candidate compounds/drugs in vitro against SSL, and furthermore confirm their efficacy in an in vivo animal model.

In the present study, we first generated SSL-specific gene signatures from DNA microarray data of SSL and normal mucosal tissues obtained from multiple patients, and identified candidate preventive compounds against SSL from 1309 compounds employing CMAP analysis. We then screened the efficacy of the candidate compounds in vitro using

patient-derived organoids of SSL (SSL-PDOs). Since we ultimately identified lansoprazole as a promising candidate drug, we then confirmed its efficacy on SSL in vivo using SSL orthotopic xenograft mice. Furthermore, we investigated the detailed mechanism of lansoprazole on SSL using SSL-PDOs.

Materials and Methods

Patients and samples

We enrolled 3 patients with SSL sized 10-20 mm to obtain 3 pairs of SSL tissue and surrounding normal colonic tissue by biopsy under colonoscopy for microarray analysis. The samples were immediately preserved in RNAlater (Sigma, St. Louis, MO) and stored at -80°C. The SSLs were then removed by endoscopic mucosal resection (EMR), and the histological diagnosis of SSL was confirmed by 2 pathologists (H.U. and Y.B.) according to WHO criteria 2019 [8]. Similarly, we enrolled 4 additional patients with SSL sized 10-20 mm and obtained SSL tissues and surrounding normal epithelia by biopsy for establishment of PDO. Patient and tumor characteristics are provided in Supplementary Figure 1a, and endoscopic and histopathological appearances are shown in Supplementary Figure 1b and 1c.

This study was approved by the Ethics Committee of Tokushima University Hospital (Approval number; 2250), and all patients gave written informed consent.

Gene signatures of sessile serrated lesions and CMAP analysis

To identify the SSL-specific gene signature, we estimated the difference in gene expression as follows. We performed the outlier test for all values of microarray probes and

calculated a z-score for each probe as previously described [24]. The z-score of each gene was then transformed into probability, and then each difference in gene probability between the 2 sets, p_k^d, was calculated, as described previously [24]. The difference in gene expression between SSL and normal tissue was estimated by the following 8 analyses. First, we selected the approximately top 200 or 1000 genes with higher p_k^d values or higher fold change, and created the 4 SSL-specific signatures, respectively. We then performed enrichment analysis on each of the 4 gene signatures in the molecular signature database (http://www.broadinstitute.org/gsea/msigdb), providing another 4 gene signatures. The enrichment probability of the gene list was estimated based on the hypergeometric probability, as previously described [25]. In the present study, we selected enriched gene sets with p values <5%. A total of 8 gene signatures were analyzed by CMAP (https://www.broadinstitute.org/connectivity-map-cmap). For each of the signatures, an enrichment score (ranging from -1 to 1) and p value for each compound were calculated by CMAP as described previously [18]; a negative enrichment score denotes an inhibitory effect of compounds on the SSL-specific signature to the normal epithelia ranking with the strongest compound designated as -1. We selected all compounds featuring a negative enrichment score and p value < 0.05 on permuted results by compound and cell line from the 8 CMAP datasets. In the case of a duplicated compound, the better (lower) enrichment score and p value were selected, and compounds that could not be practically used for long-term prophylaxis were then manually excluded. The detailed schema of drug selection based on gene profiles of SSL is shown in Figure 1b.

Compounds

Cimetidine (C4522-5G), ranitidine hydrochloride solid (R101-1G), nizatidine analytical standard (N7035-5G), naproxen sodium (M1275-5G), acetylsalicylic acid (A5376-100G), etodolac (E0516-10MG), omeprazole solid (O104-100MG), lansoprazole (L8533-250MG), chloroquine diphosphate salt (C6628-25G), disulfiram (PHR1690-1G), pyridoxine (S5669-5G), acacetin (00017-25MG), capsaicin (M2028-50MG), theobromine (T4500-25G), luteolin (L9283-10MG), guaifenesin (PHR1027-1G), gibberellic acid (G7645-500G), and tretinoin (PHR1187-3X100MG) were purchased from Sigma-Aldrich (St. Louis, MO). Lansoprazole for animal experiments was purchased from Tokyo Kasei Kogyo. Co., Ltd. (Tokyo, Japan).

Patient-derived organoid culture

Isolation of crypts and organoid cultures from biopsy specimens of human SSLs and normal colonic mucosa was performed, as described previously [26, 27].

Organoid viability assay

The viability assay for SSL-PDO and PDO of normal colonic mucosa (Nr-PDO) was performed using CellTiter-Glo assay kits (Promega, Madison, WI), as we described previously [26]. In brief, organoids mechanically dissociated by pipetting were suspended in basal culture medium with 5% Matrigel, seeded in 96-well plates, and incubated at 37°C. The next day, we added each compound at a variety of concentrations with a 1% final DMSO concentration, and the plates were incubated for 120 h. We then measured cell viability using CellTiter-Glo assay kits according to the manufacture's instruction. Dose-response curves were fitted to the luminescence signal intensities, and IC50 values were calculated by non-linear regression analysis using GraphPad Prism software (GraphPad Prism v.8.0).

Orthotopic xenograft mouse model of patient-derived organoid

All animal experiments were performed according to the guidelines of the Committee on Animal Care and Use of Tokushima University. Female NOD/Shi-scid, IL-2RγKO Jic (NOG) mice aged 6 weeks were obtained from In-Vivo Science, Inc. (Tokyo, Japan). SSL-PDOs transduced with GFP-luciferase lentivector were orthotopically transplanted into the colon of NOG mice, as previously described [23]. Briefly, mice were anesthetized and the colonic lumens were washed with PBS using a thin metallic tube. A cotton swab soaked with PBS-EDTA buffer was placed inside the colorectum for 2 min. An electric brush was then inserted into the colorectum and the ventral side of the lumen was gently rubbed. The cell suspension of organoids (1-3 × 10^6 cells/100 μL cold PBS with 15% Matrigel) was injected into the colonic lumen. The anus was sutured for 12 h and then removed.

In vivo experiment with orthotopic xenograft mice

The experimental schema of the orthotopic xenograft model is shown in Figure 4a. We generated 16 orthotopic xenograft mice of SSL-PDO and evaluated engraftment using IVIS spectrum 4 weeks after transplantation. Four of these mice had much smaller xenograft than the others, thus we randomly assigned the remaining 12 mice to treatment (n=6) and vehicle (n=6) groups. Mice in the treatment group were given 50 mg/kg of lansoprazole suspended in 0.5 % carboxymethyl cellulose (CMC), and mice in the vehicle group were given 0.5% CMC alone, using a gastric sonde, every day for 8 weeks. Luminescence images of mice in each group were obtained after intraperitoneal injection of d-luciferin using an IVIS Spectrum every week for 8 weeks, and the mice were then sacrificed for endoscopic observation and histological analysis of the xenograft colon.

Detailed methods for microarray analysis, patient-derived organoid culture, organoid size measurement, BrdU proliferation assay, lentiviral transduction, in vivo and ex vivo imaging, histological assessment, western blotting**,** cell cycle analysis, apoptosis analysis, and statistics are provided in Supplementary Methods.

Results

Generation of gene signatures of sessile serrated lesions

To generate SSL-specific gene signatures, we obtained biopsies from the SSL and the surrounding normal mucosa in each of the 3 patients showing endoscopic findings in Figure 1a. We then extracted RNA and performed microarray analysis on the extracted RNA. Based on the differential expression of genes, 8 kinds of SSL-specific gene signatures were generated using the top 200 or 1000 genes, and fold change or probability difference, and these were applied for gene set enrichment analysis (GSEA) of the signaling pathway. A representative heat map of a gene signature among 8 signatures consisting of 552 upregulated and 472 downregulated genes is provided in Figure 1c, and the 1024 gene names are listed in Supplementary Table 1. The gene list of the remaining 7 signatures are described in Supplementary Tables 2-8.

Selection of preventive candidate drugs for sessile serrated lesions using Connectivity Mapping

To identify effective compounds against SSL, we then applied SSL-specific signatures to CMAP analysis and selected 221 candidate compounds with $p<0.05$ for the enrichment score (Supplementary Tables 9-17). Of these compounds, we excluded 204 due to adverse

events, oral bioavailability and cost considering long-term oral administration, and selected the remaining 17 compounds as colorectal cancer prophylaxis candidates (Fig. 1b). The 17 compounds and respective enrichment scores are listed in Figure 1d.

Identification of effective compounds for sessile serrated lesions using human-derived organoids

To evaluate the in vitro effect of the 17 compounds selected by CMAP analysis, we established SSL-PDOs and examined their inhibitory effects on SSL-PDOs by cell viability assay (Fig. 2a). The IC50 values of 14 compounds were determined to range from 47 μM to 4902 μM, while the values were not determined for the remaining 3 compounds (Fig. 2b). Of these, lansoprazole and chloroquine showed the lowest IC50 values (47 μM and 56 μM, respectively). Therefore, viability assays were performed using SSL-PDOs obtained from 2 additional patients. The mean IC50 value of lansoprazole among the 3 PDOs was 42.5 ± 7.1 μM, whereas the mean IC50 value of chloroquine was 126 ± 50 μM (Fig. 2c). We also performed cell viability assays on Nr-PDOs after treatment with lansoprazole or vehicle alone. The percentage of viable SSL-PDO cells was significantly lower than that of viable Nr-PDO cells treated with lansoprazole at concentrations of 25 μM and 50 μM (Supplementary Fig. 2). These data suggest that lansoprazole is the best candidate for chemoprevention against SSL. Moreover, when SSL-PDO was incubated with lansoprazole (50 μM), the size of the PDOs was significantly inhibited compared with PDOs treated with vehicle alone (116.4 ± 6.2 vs. 137.2 ± 7.1 μm; $p<0.05$) (Fig. 2d, 2e). In the BrdU assay, the cell proliferation ability of SSL-PDOs was significantly suppressed in a dose-dependent manner by lansoprazole (Fig. 2f). Thus, lansoprazole exhibited the strongest inhibitory effect on SSL-PDOs among the 17 compounds. Therefore, we focused on lansoprazole in the following experiments.

Generation of an orthotopic xenograft mouse model of sessile serrated lesions

Since there have been no prior reports of an animal model of SSL, we established an orthotopic xenograft mouse model of SSL-PDO. We first transfected a lentiviral vector expressing green fluorescent protein (GFP) and firefly luciferase into SSL-PDOs, and then confirmed a green fluorescence signal in the transfected organoids (Fig. 3a). Next, these organoid cells were orthotopically transplanted into the intestinal tract of NOG mice. In the transplanted mice, clear luminescence signals were observed in the lower abdomen using the IVIS Spectrum after intraperitoneal administration of D-luciferin, and the luminescence intensity gradually increased with tumor growth every week (Fig. 3b). Five weeks after transplantation, NOG mice were sacrificed and the colons removed were excised longitudinally. The luminescence signal was observed up to about 2 cm from the anal verge after spraying D-Luciferin using the IVIS Spectrum (Fig. 3c). Autofluorescence endoscopy detected island-shaped tumor lesions with green fluorescence of GFP in the corresponding area of the colorectum, and magnified images observed under a stereomicroscope exhibited dilatation of crypt lumens in the xenograft tumor area (Fig. 3d). Histological examination of the tumor area showed dilation of the crypt base and serrations extending into the crypt base, a morphologic feature of SSL, distinct from those of surrounding normal epithelia, which was very similar to the histological findings of the same SSL specimen resected endoscopically (Fig. 3e). The xenograft area also showed a clear green fluorescence under fluorescence microscopy. These data indicated that our xenograft mouse is useful as a mouse model of SSL.

Lansoprazole inhibited development of sessile serrated lesions in xenograft mice

To evaluate the effect of lansoprazole on SSL in vivo, we administered lansoprazole (50 mg/kg p.o.) or vehicle alone to SSL-xenograft mice daily for 8 weeks, and obtained the luminescence image of mice using the IVIS Spectrum weekly (Fig. 4a). There was no significant difference in body weight during the experimental period (Supplementary Fig. 3a) and luminescence intensity at the start of treatment (Supplementary Fig. 3b) between the groups. The median value (percentage) of luminescence intensity in the lansoprazole group was marginally lower than that in control group at 8 weeks (114.8 % vs. 179.5 %; p=0.065) (Fig. 4b). Representative luminescence images of mice observed using the IVIS Spectrum in each group are shown in Supplementary Figure 3c. Autofluorescence endoscopy identified smaller fluorescent lesions in the colorectum of the lansoprazole group as compared with the control group, as shown in the respective representative images (Fig. 4c). Histological examination revealed similar appearance of green fluorescence in the xenograft lesion from the lansoprazole and control groups, but the Ki67-positive cells in the xenograft lesions from the lansoprazole group was obviously fewer than in the control group, as shown in the respective representative images (Fig. 4d). The median value of Ki67 index in the lansoprazole group was significantly lower than in the control group (29.7% vs. 49.6%; $p<0.05$) (Fig. 4e). On the other hand, no significant difference in Ki-67 index of normal mice colon epithelium surrounding the xenograft was observed between lansoprazole and control (vehicle) mouse groups (Supplementary Fig. 4). Thus, lansoprazole suppressed the proliferation of SSL cells in xenograft mice.

Lansoprazole affected cell cycle-related pathways in sessile serrated lesions

To investigate the mechanism of the inhibitory effect of lansoprazole on SSL cell proliferation, we performed microarray analysis of the 3 SSL-PDOs treated with lansoprazole (100 μM) or vehicle alone, and compared gene expression profiles between

them to generate a lansoprazole-specific signature. The lansoprazole-specific signature consisted of 459 upregulated and 379 downregulated genes with p_k^d >0.1, and the list of these 838 genes is shown in Supplementary Table 18. The GSEA of those genes yielded 174 pathways (p<0.05), which are listed in Supplementary Table 19. The top 20 pathways with the lowest p values for the lansoprazole-specific signature are shown in Figure 5a; many cell cycle-related pathways were identified, which are associated with cell growth inhibition of SSL. When the expression of individual genes in the KEGG cell cycle pathway was examined in the lansoprazole-treated PDOs, 4 upregulated and 21 downregulated genes with p_k^d value > 0.1 were identified (Fig. 5b).

Effects of lansoprazole on molecules related to cell cycle arrest

Since the microarray analysis suggested a strong effect of lansoprazole on the cell cycle in SSL cells, we analyzed the cell cycle change and related proteins in SSL-PDOs. First, we examined the cell cycle histogram of SSL-PDOs after treatment with lansoprazole or vehicle for 0-24 h by flow cytometry. The histogram of lansoprazole-treated SSL-PDOs at 24 h exhibited an increase in the G1 phase and a decrease in the S and G2/M phases (Fig. 5c). Quantitative analysis showed significantly higher G1 phase cells and lower S and G2/M phase cells in lansoprazole-treated SSL-PDOs at 18 h and 24 h (Fig. 5d). However, no significant change in the number of G1, S, or G2/M phase cells was observed in lansoprazole-treated Nr-PDO compared with vehicle-treated Nr-PDO at 24 h (Supplementary Fig. 5). These data suggest that lansoprazole inhibits cell proliferation of SSL by inducing G1 arrest. Among the 25 lansoprazole-specific genes in the cell cycle pathway (Fig. 5b), S-phase kinase associated protein 2 (Skp2), CDKN1B (p27), CDK2, and CCNE (cyclin E) are reported to be associated with G1 arrest. Western blot analysis revealed that the protein expression level of Skp2, a degradation protein of p27, was

downregulated in the lansoprazole-treated SSL-PDO. The expression of p27 was upregulated in the lansoprazole-treated SSL-PDO. In addition, the expression of CDK2 and cyclin E1, which are regulated by p27 and directly trigger the G1-S phase transition, were downregulated in the lansoprazole-treated SSL-PDO (Fig. 5e).

We then examined apoptotic cell death of SSL-PDOs after treatment with lansoprazole by flow cytometric analysis of annexin V. The percentage of annexin V-positive cells (apoptotic cells) was increased by lansoprazole in a dose dependent manner (Supplementary Fig. 6a, 6b). Regarding stemness induction, although we checked mRNA levels of 13 stemness markers in SSL-PDOs treated with lansoprazole or vehicle alone on the basis of microarray analysis data, none of the 13 markers were increased in SSL-PDO treated with lansoprazole (Supplementary Fig. 6c). These data suggest that lansoprazole inhibits SSL proliferation by inducing G1 arrest via downregulation of Skp2 and upregulation of p27, and then underwent apoptotic cell death (Fig. 5f).

Discussion

In this study, we selected 17 candidate chemopreventive compounds among 1309 FDA-approved compounds as candidates to investigate for the prevention of SSL employing CMAP analysis, and ultimately identified lansoprazole as the most effective compound based on in vitro evaluation using SSL-PDOs. We also demonstrated the inhibitory effect of lansoprazole on SSL in vivo using a mouse model involving orthotopic xenotransplantation of SSL-PDOs. Furthermore, we revealed the mechanism of the inhibitory effect of lansoprazole, which downregulated Skp2 expression and thereby activated p27, leading to G1 arrest of the cells. This is the first study to comprehensively analyze numerous compounds/drugs using SSL gene profiles and CMAP data, and to confirm their inhibitory effects in vitro and in vivo by applying SSL-PDOs and animal models.

Lansoprazole is an FDA-approved proton pump inhibitor (PPI), which is used for treatment of acid-related disorders including gastroesophageal reflux disease, peptic ulcer, and Zollinger-Ellison syndrome. No clinical study showing an inhibitory effect of lansoprazole or other PPIs on SSL has been reported to date. However, there has been a single retrospective observational study showing that long-term oral administration of PPIs including lansoprazole and omeprazole reduced the number of HPs [28]. Our study showed an inhibitory effect of lansoprazole on SSLs, which is not on HPs. However, in this study, not only lansoprazole but also omeprazole was identified as a candidate compound and showed a relatively low IC50 value (Fig. 2b). Because SSL and HP are histologically similar to each other, their study may support our findings regarding lansoprazole. In addition, aspirin and NSAIDs (naproxen, etodolac) were selected as candidate compounds for the prevention of SSL based on CMAP analysis. This finding is consistent with previous reports indicating that aspirin or NSAIDs may be effective in the prevention of serrated polyps [16, 29]. However, in our study, aspirin, naproxen and etodolac showed relatively higher IC50 values (4902 μM, 614 μM, and 708 μM, respectively), whereas lansoprazole showed a much lower IC50 value (47 μM), suggesting that lansoprazole is even more effective than aspirin or NSAIDs against SSLs.

In the present study, we reported for the first time an orthotopic xenograft mouse model of human SSL using organoids established from biopsy specimens of patients. There have been several studies on mouse models of serrated CRC [30-32], but no animal model of precancerous SSL has been reported so far. Bond et al. reported Braf mutant mice which developed serrated lesions in the small intestine by 8 months [33]. However, no colonic lesion developed in their model, and it is not clear whether the serrated lesions in the small intestine are indeed precancerous lesions which are similar to colonic SSL in humans. In contrast, the tumor in our mouse model was located in the colon and its pathological

features were identical to those of SSL in humans. These findings suggest that our model is very useful for evaluating agents for the prevention of human SSL.

We evaluated the in vivo effect of lansoprazole against SSL in mice at a dose of 50 mg/kg/day for 8 weeks. Although the bioluminescence intensity in the lansoprazole-treated group was lower than in the vehicle group, the difference was marginally significant but not statistically significant (114.8% vs 179.5%; p=0.065). We speculate the following possibilities as the underlying reasons. 1) Although we designed an in vivo treatment protocol lasting 8 weeks, the duration of treatment might have been too short to lead to a significant difference because the growth rate of SSL tumors was very low. In fact, tumor volume in our SSL-xenograft mice (vehicle group) at 12 weeks was only 1.5 times greater than that at 4 weeks although the xenograft of colon cancer PDO reportedly showed a 3-fold increase in tumor volume for 60 days [34]. This slow growth rate of SSL tumor might have resulted in an inadequate duration of lansoprazole treatment. 2) The oral dose of lansoprazole administered to mice might have been insufficient, as suggested by a previous study showing a difference in metabolism of lansoprazole between mice and humans [35]. However, we found that the number of Ki-67 positive cells per tumor area in mice treated with lansoprazole, which is a well-known indicator of proliferative potential, was significantly lower than that of mice treated with vehicle alone, as revealed by immunofluorescence. Based on these data, we would expect that long-term administration of the drug would provide significant tumor inhibition in vivo.

We found lansoprazole among 1309 compounds using the SSL-specific signature, and clarified its mechanism of tumor inhibition using the lansoprazole-specific signature obtained from SSL-PDO after treatment with lansoprazole. Theoretically, the SSL-specific signature and lansoprazole-specific signature would be expected to be similar. When these 2 signatures were compared, some percentage of the genes and pathways were commonly

identified in both signatures (Supplementary Tables 20-22). However, some of the genes and pathways were not found in the other signature, suggesting a discrepancy between them. This discrepancy may be explained by the fact that SSL-specific signatures were generated by comparing gene expression between human SSL and normal colorectal tissue obtained by biopsy during colonoscopy, whereas lansoprazole-specific signature was generated by comparing between SSL-PDO treated with lansoprazole and vehicle alone in vitro, which comprised only SSL cells without stroma.

In the present study, we first found that lansoprazole downregulated Skp2 expression and upregulated p27 expression, leading to G1 phase cell cycle arrest. Skp2 is upregulated in a variety of cancers, including CRC, and is thought to contribute to tumor progression [36]. Although there have been no previous reports showing that lansoprazole or other PPIs induced downregulation of Skp2 expression in cancers, several studies have shown that PPIs, including lansoprazole, have antitumor effects against several kinds of cancers [37-42]. Omeprazole inhibited growth in human colon cancer cell lines via induction of $p21^{waf1/cip1}$ [39] and lansoprazole induces cell cycle arrest via upregulation of $p27^{kip1}$ in lung cancer cell lines [42]. Since Skp2 leads to downregulation of p27 and p21 by ubiquitination and degradation, these reports suggest that Skp2 may be involved in the inhibitory effect of lansoprazole not only in SSL but also in some cancers. However, the progression of SSL involves a loss of function of a cell cycle-dependent kinase inhibitor [30], which represents a state of suppressed cell cycle arrest. Therefore, this inhibitory mechanism of lansoprazole may be compatible with those previous studies.

In general, lansoprazole as a proton-pump inhibitor, is a prodrug, which converts to an active form under acidic conditions, and it inhibits acid secretion by binding to sulfhydryl group in the H^+/K^+-ATPase. It has been reported that ATP4A, ATP4B, and ATP12A genes, which encode H+/K+-ATPase, are not expressed in normal colonic mucosa or colorectal

cancer in the Human Protein Atlas (https://www.proteinatlas.org). We also confirmed no expression of these genes in SSL as well as in normal colorectal tissues on the basis of our microarray data (Supplementary table 1-8). On the other hand, recent studies reported that PPIs including lansoprazole suppress cancer cell growth by inhibiting vacuolar-type ATPase (V-ATPase) [37, 38]. Moreover, Zeng et al. reported that cancer cell growth was inhibited by pantoprazole in medium with pH 7.2-7.4, not under acid conditions, and noted that pantoprazole inhibits colorectal cancer growth in its prodrug form (pantoprazole) [41]. Similarly, in this study, we confirmed that lansoprazole strongly inhibited cell growth of SSL-PDOs in vitro in non-acidic conditions (pH 7.2-7.4). Therefore, we speculate that lansoprazole inhibits proliferation of SSL by its prodrug form regardless of the inhibition of proton pump function.

In the present study, we used CMAP to comprehensively select an effective compound against SSL from a large number of agents. Because CMAP is based on data of preexisting compounds, selected compounds can be studied immediately in clinical chemoprevention trials. Patients who undergo endoscopic resection of large SSLs reportedly have a high risk of CRC [43]. Moreover, serrated polyposis syndrome is well documented as the most common gastrointestinal polyposis syndrome (gastrointestinal polyposis syndrome with the highest prevalence), and it predisposes patients to a high risk of CRC (15.3%-24.5%) [44]. It is very important to prevent the development of CRC in such patients. Lansoprazole appears to be an ideal drug for these patients due to its low cost and high safety.

One of limitations in this study is that the sample size to generate SSL-specific gene signatures was relatively small. We compared our transcriptome data for SSL in this study with those in a previous study, which showed 1000 genes specifically upregulated and downregulated in SSL from 10 pairs of tumor and normal colonic tissues [45], and found that our SSL-specific signatures were mostly consistent with those reported previously.

Another limitation in this study is that the sample size of animal experiments was relatively small. Therefore, it would be important to confirm the data using a larger number of animals with the SSL xenograft model concomitant with a longer duration of lansoprazole treatment.

In conclusion, this is the first study to comprehensively analyze compounds for the chemoprevention of SSL, employing CMAP analysis, SSL-PDOs, and an orthotopic xenograft mouse model. Our data demonstrate that lansoprazole is the most effective agent for SSL chemoprevention among 1309 FDA-approved compounds, and that lansoprazole induces G1 arrest in SSL cells via Skp2 downregulation.

Acknowledgements: The authors would like to thank Drs. Hisanori Uehara and Yoshimi Bando (Department of Pathology, Tokushima University Hospital) for their support of pathological diagnosis. We are also grateful to Ms. Hiroko Nakanishi (Department of Gastroenterology and Oncology, Tokushima University Graduate School) for the assistance of experiments.

Author contributions: Conceptualization: TK, KO, NM, TT. Data curation: TK, SF, MB, HW. Investigation: TK, KO, SF, MB, HW, HM, YS, NM, TT. Methodology: TK, KO, NM, TT. Formal analysis: KH. Writing-original draft: TK, KO, TT. Writing-review & editing: TK, KO, TT. Funding acquisition: TT.

Funding: This work was partly funded by JSPS KAKENHI, a grant number 17H01463.

Declarations

Conflict of interest: The authors have no conflicts of interest to disclose.

Data availability: Most of the data are provided in supplementary materials. The remaining data will be shared on reasonable request addressed to takayama@tokushima-u.ac.jp.

References

1. Bray F, Ferlay J, Soerjomataram I, et al. Global cancer statistics 2018: GLOBOCAN estimates of incidence and mortality worldwide for 36 cancers in 185 countries. CA Cancer J Clin. 2018;68:394-424.
2. Vogelstein B, Fearon ER, Hamilton SR, et al. Genetic Alterations during Colorectal-Tumor Development. N Engl J Med. 1988;319:525-32.
3. Leggett B, Whitehall V. Role of the Serrated Pathway in Colorectal Cancer Pathogenesis. Gastroenterology. 2010;138:2088-100.
4. Snover DC. Update on the serrated pathway to colorectal carcinoma. Hum Pathol. 2011;42:1-10.
5. Sweetser S, Smyrk TC, Sinicrope FA. Serrated Colon Polyps as Precursors to Colorectal Cancer. Clin Gastroenterol Hepatol. 2013;11:760-7.
6. Sugai T, Habano W, Takagi R, et al. Analysis of molecular alterations in laterally spreading tumors of the colorectum. J Gastroenterol. 2017;52:715-23.
7. Jass JR. Classification of colorectal cancer based on correlation of clinical, morphological and molecular features. Histopathology. 2007;50:113-30.
8. Pai RK, Mäkinen MJ M, Rosty C. Colorectal serrated lesions and polyps. In: WHO Classification of Tumours Editorial Board (Ed.) WHO Classification of Tumours of the Digestive System. Lyon: IARC; 2019. pp.163-9.
9. Kambara T. BRAF mutation is associated with DNA methylation in serrated polyps and cancers of the colorectum. Gut. 2004;53:1137-44.
10. Higuchi T, Sugihara K, Jass JR. Demographic and pathological characteristics of serrated polyps of colorectum. Histopathology. 2005;47:32-40.
11. O'Brien MJ, Yang S, Mack C, et al. Comparison of Microsatellite Instability, CpG Island Methylation Phenotype, BRAF and KRAS Status in Serrated Polyps and

Traditional Adenomas Indicates Separate Pathways to Distinct Colorectal Carcinoma End Points. Am J Surg Pathol. 2006;30:1491-501.

12. Rosty C, Hewett DG, Brown IS, et al. Serrated polyps of the large intestine: current understanding of diagnosis, pathogenesis, and clinical management. J Gastroenterol. 2013;48:287-302.
13. Guinney J, Dienstmann R, Wang X, et al. The consensus molecular subtypes of colorectal cancer. Nat Med. 2015;21:1350-6.
14. Aderka D, Stintzing S, Heinemann V. Explaining the unexplainable: discrepancies in results from the CALGB/SWOG 80405 and FIRE-3 studies. Lancet Oncol. 2019;20:e274-e83.
15. Lenz H-J, Ou F-S, Venook AP, et al. Impact of Consensus Molecular Subtype on Survival in Patients With Metastatic Colorectal Cancer: Results From CALGB/SWOG 80405 (Alliance). J Clin Oncol. 2019;37:1876-85.
16. Wallace K, Grau MV, Ahnen D, et al. The association of lifestyle and dietary factors with the risk for serrated polyps of the colorectum. Cancer Epidemiol Biomarkers Prev. 2009;18:2310-7.
17. Jass JR, Whitehall VL, Young J, et al. Emerging concepts in colorectal neoplasia. Gastroenterology. 2002;123:862-76.
18. Lamb J. The Connectivity Map: Using Gene-Expression Signatures to Connect Small Molecules, Genes, and Disease. Science. 2006;313:1929-35.
19. Jin L, Tu J, Jia J, et al. Drug-repurposing identified the combination of Trolox C and Cytisine for the treatment of type 2 diabetes. J Transl Med. 2014;12:153.
20. Shigemizu D, Hu Z, Hung J-H, et al. Using Functional Signatures to Identify Repositioned Drugs for Breast, Myelogenous Leukemia and Prostate Cancer. PLoS Comput Biol. 2012;8:e1002347.

21. Musa A, Ghoraie LS, Zhang S-D, et al. A review of connectivity map and computational approaches in pharmacogenomics. Brief Bioinform. 2018;19:506-23
22. Sato T, Stange DE, Ferrante M, et al. Long-term expansion of epithelial organoids from human colon, adenoma, adenocarcinoma, and Barrett's epithelium. Gastroenterology. 2011;141:1762-72.
23. Sugimoto S, Ohta Y, Fujii M, et al. Reconstruction of the Human Colon Epithelium In Vivo. Cell Stem Cell. 2018;22:171-6 e5.
24. Kagamu H, Kitano S, Yamaguchi O, et al. CD4(+) T-cell Immunity in the Peripheral Blood Correlates with Response to Anti-PD-1 Therapy. Cancer Immunol Res. 2020;8:334-44.
25. Kosaka T, Nagamatsu G, Saito S, et al. Identification of drug candidate against prostate cancer from the aspect of somatic cell reprogramming. Cancer Sci. 2013;104:1017-26.
26. Wada H, Sato Y, Fujimoto S, et al. Resveratrol inhibits development of colorectal adenoma via suppression of LEF1; comprehensive analysis with connectivity map. Cancer Sci. 2022;113:4374-84.
27. Takahashi S, Okamoto K, Tanahashi T, et al. S100P Expression via DNA Hypomethylation Promotes Cell Growth in the Sessile Serrated Adenoma/Polyp-Cancer Sequence. Digestion. 2021;102:789-802.
28. Singh M, Dhindsa G, Friedland S, et al. Long-term use of proton pump inhibitors does not affect the frequency, growth, or histologic characteristics of colon adenomas. Aliment Pharmacol Ther. 2007;26:1051-61.
29. Johnson CC, Hayes RB, Schoen RE, et al. Non-Steroidal Anti-Inflammatory Drug Use and Colorectal Polyps in the Prostate, Lung, Colorectal, and Ovarian Cancer Screening Trial. Am J Gastroenterol. 2010;105:2646-55.

30. Carragher LA, Snell KR, Giblett SM, et al. V600EBraf induces gastrointestinal crypt senescence and promotes tumour progression through enhanced CpG methylation of p16INK4a. EMBO Mol Med. 2010;2:458-71.
31. Sakamoto N, Feng Y, Stolfi C, et al. BRAF(V600E) cooperates with CDX2 inactivation to promote serrated colorectal tumorigenesis. eLife. 2017;6:e20331.
32. Lannagan TRM, Lee YK, Wang T, et al. Genetic editing of colonic organoids provides a molecularly distinct and orthotopic preclinical model of serrated carcinogenesis. Gut. 2019;68:684-92.
33. Bond CE, Liu C, Kawamata F, et al. Oncogenic BRAF mutation induces DNA methylation changes in a murine model for human serrated colorectal neoplasia. Epigenetics. 2018;13:40-8.
34. Shimokawa M, Ohta Y, Nishikori S, et al. Visualization and targeting of LGR5(+) human colon cancer stem cells. Nature. 2017;545:187-92.
35. Kikuchi H, Kato H, Mizuno M, et al. Differences in Inducibility of CYP1A1-mRNA by Benzimidazole Compounds between Human and Mouse Cells: Evidences of a Human-Specific Signal Transduction Pathway for CYP1A1 Induction. Arch biochem biophys. 1996;334:235-40.
36. Hume S, Grou CP, Lascaux P, et al. The NUCKS1-SKP2-p21/p27 axis controls S phase entry. Nat Commun. 2021;12:6959.
37. Luciani F, Spada M, De Milito A, et al. Effect of Proton Pump Inhibitor Pretreatment on Resistance of Solid Tumors to Cytotoxic Drugs. J Natl Cancer Inst. 2004;96:1702-13.
38. De Milito A, Canese R, Marino ML, et al. pH-dependent antitumor activity of proton pump inhibitors against human melanoma is mediated by inhibition of tumor acidity. Int J Cancer. 2010;127:207-19.

39. Patlolla JM, Zhang Y, Li Q, et al. Anti-carcinogenic properties of omeprazole against human colon cancer cells and azoxymethane-induced colonic aberrant crypt foci formation in rats. Int J Oncol. 2012;40:170-5.

40. Zhang S, Wang Y, Li SJ. Lansoprazole induces apoptosis of breast cancer cells through inhibition of intracellular proton extrusion. Biochem Biophys Res Commun. 2014;448:424-9.

41. Zeng X, Liu L, Zheng M, et al. Pantoprazole, an FDA-approved proton-pump inhibitor, suppresses colorectal cancer growth by targeting T-cell-originated protein kinase. Oncotarget. 2016;7:22460-73.

42. Zhao X, Zhang N, Huang Y, et al. Lansoprazole Alone or in Combination With Gefitinib Shows Antitumor Activity Against Non-small Cell Lung Cancer A549 Cells in vitro and in vivo. Front Cell Dev Biol. 2021;9:655559.

43. He X, Hang D, Wu K, et al. Long-term Risk of Colorectal Cancer After Removal of Conventional Adenomas and Serrated Polyps. Gastroenterology. 2020;158:852-61 e4.

44. Muller C, Yamada A, Ikegami S, et al. Risk of Colorectal Cancer in Serrated Polyposis Syndrome: A Systematic Review and Meta-analysis. Clin Gastroenterol Hepatol. 2022;20:622-30

45. Ohki D, Yamamichi N, Sakaguchi Y, et al. Transcriptome of sessile serrated adenoma/polyps is associated with MSI-high colorectal cancer and decreased expression of CDX2. Cancer Med. 2022;11:5066-78.

Figure legends

Fig. 1 Generation of sessile serrated lesion (SSL)-specific gene signature and selection of candidate compounds for cancer prevention from Connectivity Map analysis. **a** Endoscopic images of SSLs from which biopsy tissue was taken for DNA microarray analysis. **b** Flowchart for compound selection. Four SSL-specific signatures consisted of the top 208 to 1045 genes based on 2 mathematical analysis methods; higher fold change (fc) or higher p_k^d (pd) values. GSEA was performed on each signature to generate 4 additional signatures. The compounds were selected by employing CMAP analysis based on a total of the 8 signatures. Compounds unsuitable for long-term administration were excluded. **c** Representative heat map image describing the top 1024 genes with high fc derived from microarray data of SSLs and corresponding normal mucosae of 3 individual cases. Green indicates genes with low expression levels and red indicates genes with high expression levels. **d** A list of 17 candidate compounds and their enrichment scores and p values calculated by CMAP analysis based on SSL-specific gene signatures.

Fig. 2 Preventive compound screening by evaluating inhibitory effect on patient derived organoids (PDOs) of SSL. **a** Dose response curves of SSL-PDOs treated with each of the candidate compounds for 120 h. Organoid viability was assessed by CellTiter-Glo assay. **b** IC50 values of 17 compounds against SSL-PDOs. **c** Dose response curves of 3 individual SSL-PDOs treated with lansoprazole (left) or chloroquine (right). The mean ± SD was plotted (n = 3). **d** Microscopic images treated with vehicle alone or 50 μM lansoprazole (LPZ) for 0 h or 120 h. Scale bar, 400 μm. **e** The diameter of PDO-cluster in each group (mean ± SD). *p < 0.05 by Student's t test. F) BrdU uptake of SSL-PDOs treated with 0, 25, 50, or 100 μM lansoprazole for 24 h as shown by BrdU (ELISA) assay. Data shown is mean ± SD of n = 6. *p < 0.05, **p < 0.01 by Dunnett's test.

Fig. 3 Development of an orthotopic xenograft mouse model of organoids derived from human sessile serrated lesions. **a** Bright-field, GFP fluorescence and their merged microscopic images of SSL-PDOs infected with CMV-GFP-T2A-luciferase lentivirus. Scale bar, 100 μM. **b** Bioluminescence (IVIS) images of the xenograft mouse model obtained once a week until 5 weeks after transplantation of transfected SSL-PDOs. Red circles are the regions of interest with a diameter of 20 mm. **c** Photographic (left) and bioluminescence (right) images of the longitudinally excised colon from SSL xenograft mice. **d** Endoscopic image of the excised colon visualized with white light (left) and autofluorescence (middle) using autofluorescence image (AFI) endoscopy. Scale bar, 2 mm. A magnified image of yellow square is shown in the right panel. Right side of the image shows xenograft area and left side shows recipient area. **e** Microscopic images of xenograft area in mouse model and the adjacent recipient area of normal mouse colon, and SSL specimens endoscopically resected and used for the xenograft. Upper row shows hematoxylin and eosin (H&E) staining, and lower shows GFP fluorescence images. Scale bar, 100 μm.

Fig. 4 Growth inhibitory effect of lansoprazole on sessile serrated lesions in xenograft mice. **a** Schema of the treatment schedule for lansoprazole against SSL in vivo. **b** Bioluminescent intensity of tumors in xenograft mice up to 8 weeks after administration of lansoprazole or vehicle alone. The intensity was calculated as a percentage compared to pretreatment. Data shown are mean ± SE of n = 6. **c** Representative endoscopic autofluorescence image of tumor in xenograft of lansoprazole and vehicle group ex vivo. **d** Representative microscopic images of GFP fluorescence and Ki67 immunohistochemistry in tumors of lansoprazole and vehicle groups (dotted square). **e** Ki67 index in tumors of lansoprazole

and vehicle groups. Ki67 index is shown as a percentage of Ki67 immunostaining positive cells among GFP-positive cells. *p < 0.05 by Mann-Whitney U-test.

Fig. 5 Lansoprazole inhibits the cell cycle of patient-derived organoids of sessile serrated lesions via downregulation of Skp2 leading to G1 arrest. **a** Top 20 significantly different pathways in MsigDB comparing microarray data of SSL-PDOs treated with lansoprazole and vehicle alone. **b** A heatmap displaying upregulated and downregulated genes in KEGG cell cycle pathway in each of SSL-PDOs. **c** Representative histograms of flowcytometric analysis of SSL-PDOs treated with lansoprazole (100 μM) or vehicle alone. **d** The distribution of each cell cycle phase in SSL-PDOs treated with lansoprazole or vehicle alone for 0, 12, 18, 24 h was analyzed (n=3). **p < 0.01 by Student's t test. **e** Expression of Skp2, p27, CDK2 and cyclin E1 protein in SSL-PDOs treated with lansoprazole (50 μM) or vehicle alone for 24 h as determined by western blotting. Relative expression was calculated as a ratio of the expression level of β-actin. **f** Schema of a putative mechanism of the inhibitory effect of lansoprazole against SSL. Lansoprazole downregulated Skp2 expression, thereby activating p27, which in turn downregulated CDK2 and cyclin E, leading to G1 arrest of the cells.

a

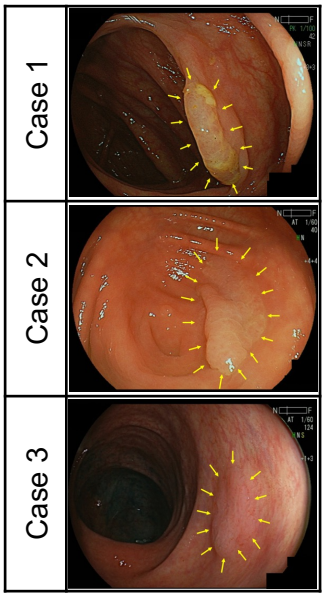

b

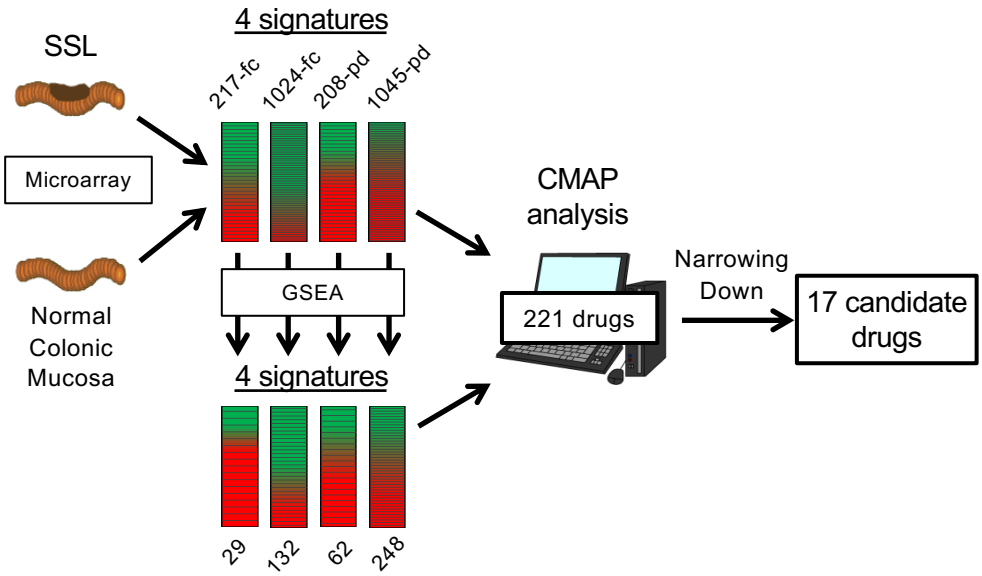

c

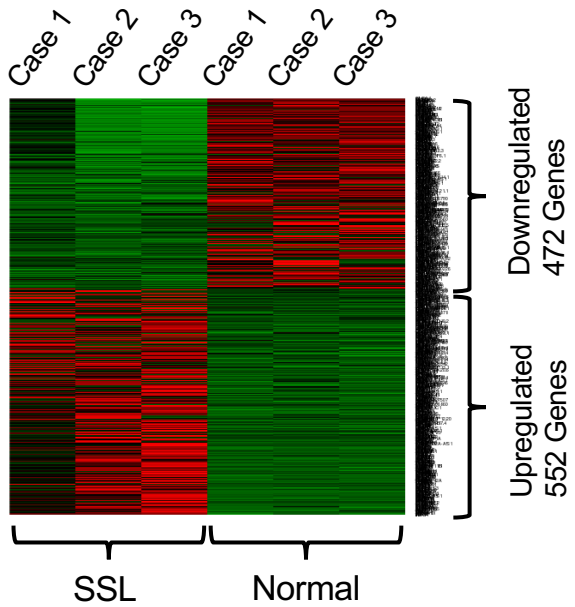

d

Compounds	Enrichment Score	*P* value
Acacetin	-0.985	0.0004
Chloroquine	-0.97	0.00176
Disulfiram	-0.966	0.00226
Pyridoxine	-0.942	0.00732
Etodolac	-0.931	0.0091
Cimetidine	-0.929	0.01096
Nizatidine	-0.925	0.01107
Naproxen	-0.91	0.01512
Theobromine	-0.91	0.0158
Luteolin	-0.898	0.01998
Ranitidine	-0.882	0.02945
Acetylsalicylic acid	-0.879	0.02862
Capsaicin	-0.877	0.03016
Omeprazole	-0.877	0.03175
Lansoprazole	-0.864	0.03634
Guaifenesin	-0.835	0.00921
Tretinoin	-0.662	0.02926

a

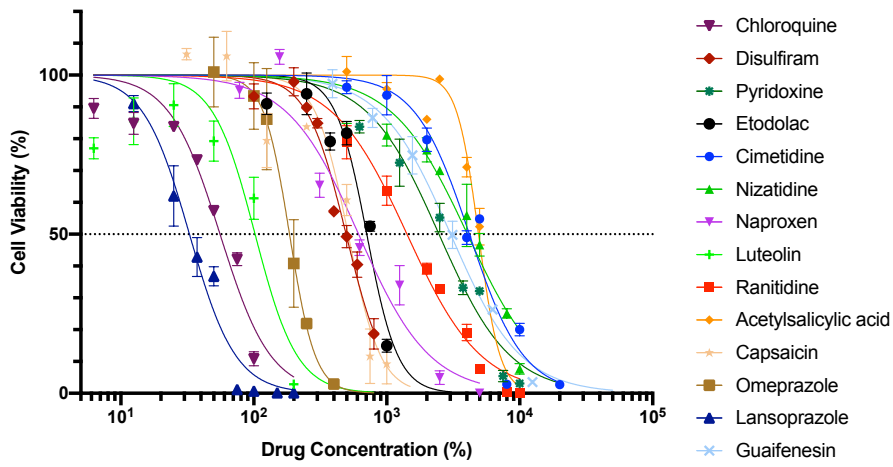

b

Compounds	IC50 (95% CI) [μM]
Acacetin	>200
Chloroquine	**56** (50.7-61.1)
Disulfiram	494 (468-523)
Pyridoxine	2471 (2156-2805)
Etodolac	708 (654-763)
Cimetidine	4182 (3644-4739)
Nizatidine	4044 (3490-4651)
Naproxen	614 (511-739)
Theobromine	>2000
Luteolin	123 (79-125)
Ranitidine	1448 (1280-1565)
Acetylsalicylic acid	4902 (4663-5159)
Capsaicin	512 (414-590)
Omeprazole	186 (166-206)
Lansoprazole	**47** (29.5-36.2)
Guaifenesin	3024 (2697-3387)
Tretinoin	Not determined

c

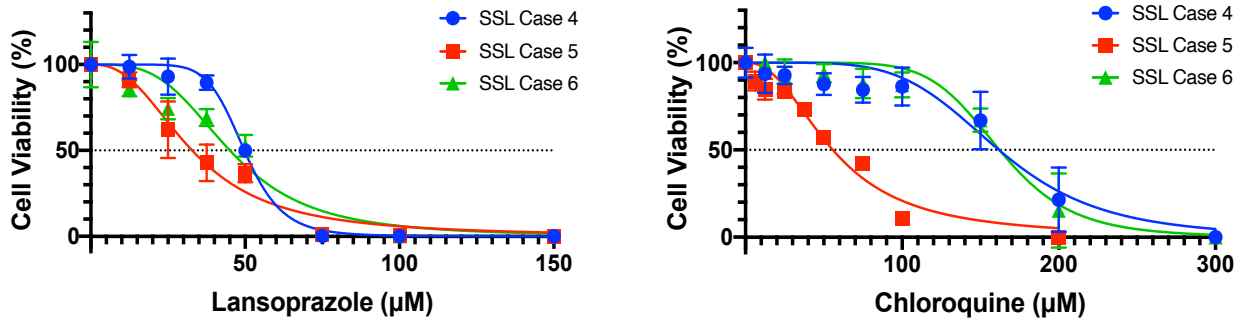

d

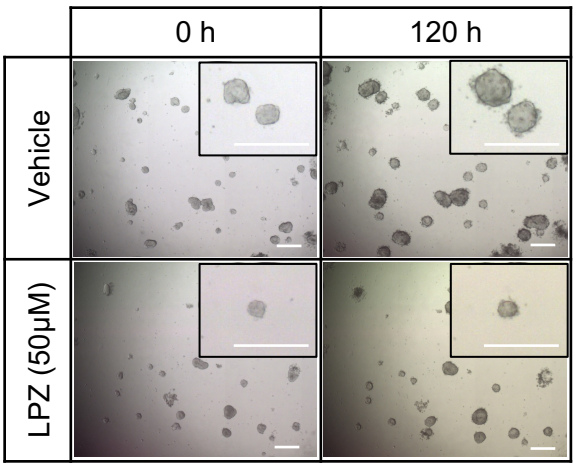

e

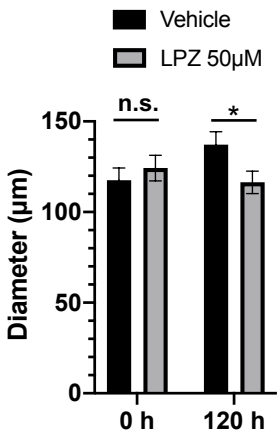

f

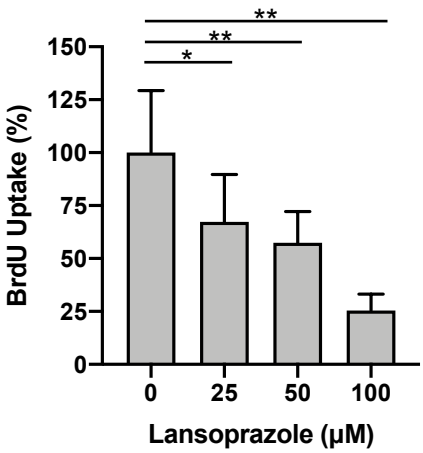

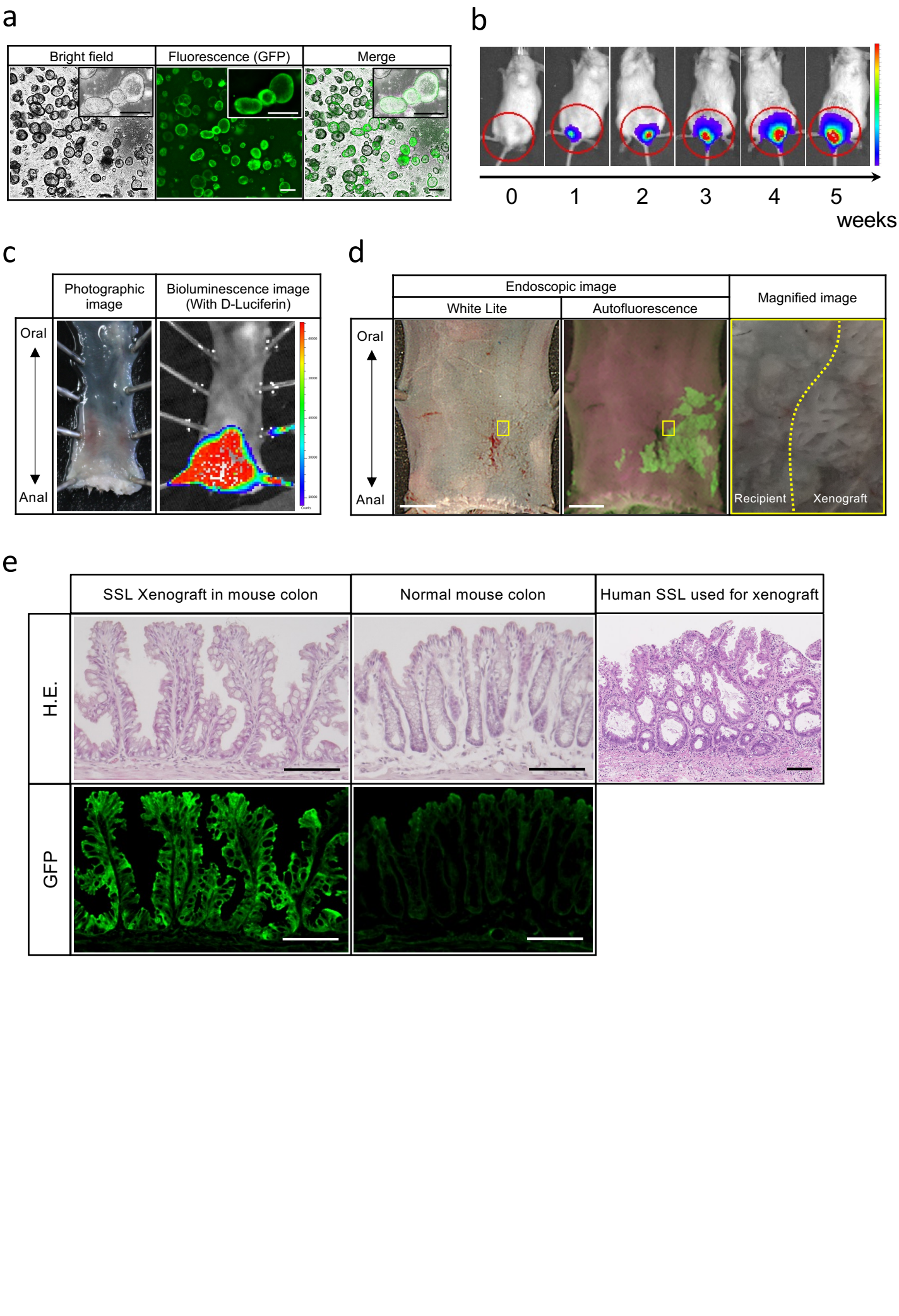
a
Bright field
Fluorescence (GFP)
Merge
b
0
1
2
3
4
5
weeks
c
Photographic image
Bioluminescence image (With D-Luciferin)
Oral
Anal
d
Endoscopic image
White Lite
Autofluorescence
Magnified image
Oral
Anal
Recipient
Xenograft
e
SSL Xenograft in mouse colon
Normal mouse colon
Human SSL used for xenograft
H.E.
GFP

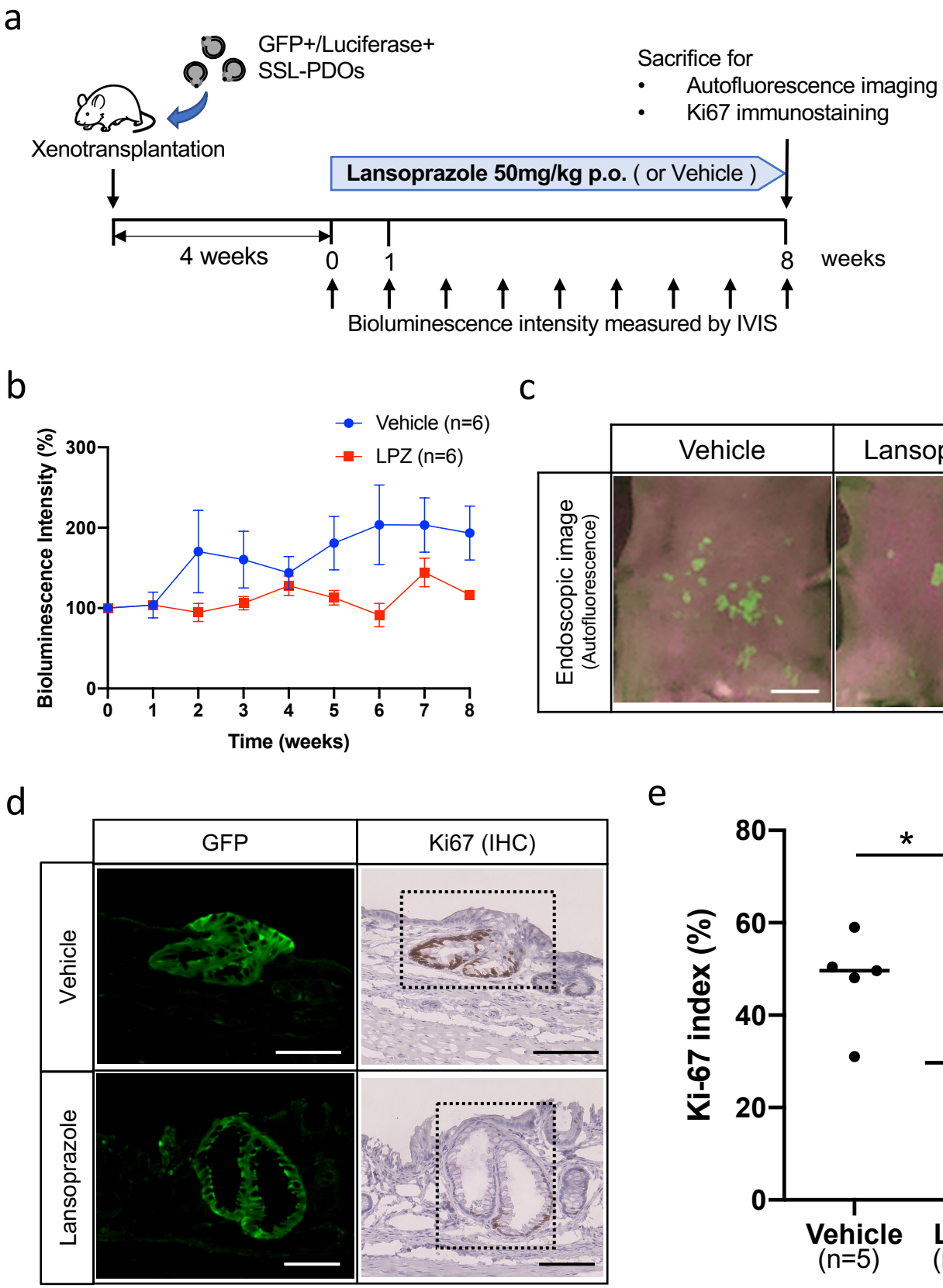
a
GFP+/Luciferase+
SSL-PDOs
Xenotransplantation
Sacrifice for
• Autofluorescence imaging
• Ki67 immunostaining
Lansoprazole 50mg/kg p.o. (or Vehicle)
4 weeks
0
1
8
weeks
Bioluminescence intensity measured by IVIS
b
Vehicle (n=6)
LPZ (n=6)
Bioluminescence Intensity (%)
300
200
100
0
0 1 2 3 4 5 6 7 8
Time (weeks)
c
Vehicle
Lansoprazole
Endoscopic image
(Autofluorescence)
d
GFP
Ki67 (IHC)
Vehicle
Lansoprazole
e
Ki-67 index (%)
80
60
40
20
0
*
Vehicle
(n=5)
LPZ
(n=6)

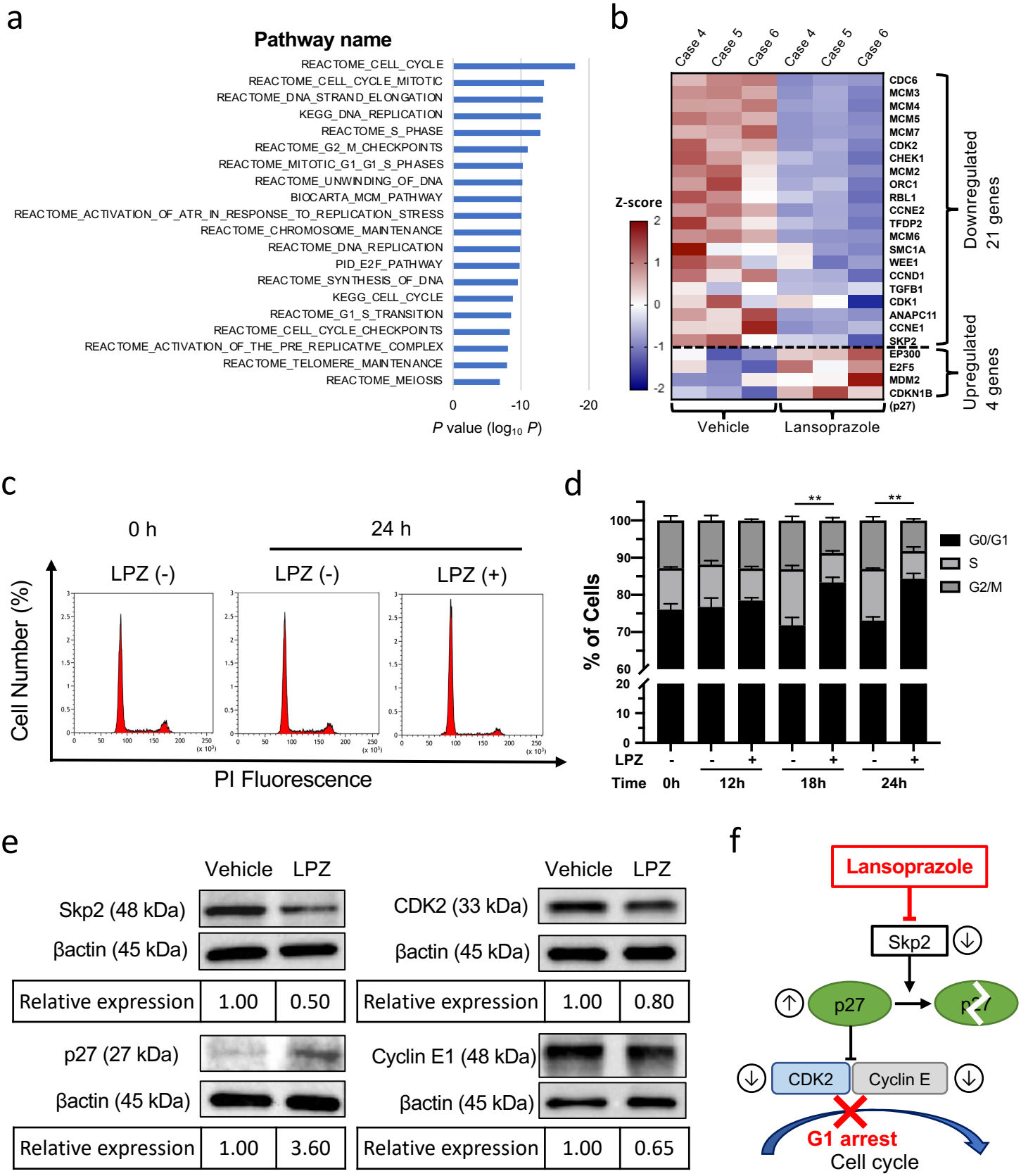
a
Pathway name
REACTOME_CELL_CYCLE
REACTOME_CELL_CYCLE_MITOTIC
REACTOME_DNA_STRAND_ELONGATION
KEGG_DNA_REPLICATION
REACTOME_S_PHASE
REACTOME_G2_M_CHECKPOINTS
REACTOME_MITOTIC_G1_G1_S_PHASES
REACTOME_UNWINDING_OF_DNA
BIOCARTA_MCM_PATHWAY
REACTOME_ACTIVATION_OF_ATR_IN_RESPONSE_TO_REPLICATION_STRESS
REACTOME_CHROMOSOME_MAINTENANCE
REACTOME_DNA_REPLICATION
PID_E2F_PATHWAY
REACTOME_SYNTHESIS_OF_DNA
KEGG_CELL_CYCLE
REACTOME_G1_S_TRANSITION
REACTOME_CELL_CYCLE_CHECKPOINTS
REACTOME_ACTIVATION_OF_THE_PRE_REPLICATIVE_COMPLEX
REACTOME_TELOMERE_MAINTENANCE
REACTOME_MEIOSIS
0
-10
-20
P value (log10 P)
b
Case 4
Case 5
Case 6
Case 4
Case 5
Case 6
Z-score
2
1
0
-1
-2
CDC6
MCM3
MCM4
MCM5
MCM7
CDK2
CHEK1
MCM2
ORC1
RBL1
CCNE2
TFDP2
MCM6
SMC1A
WEE1
CCND1
TGFB1
CDK1
ANAPC11
CCNE1
SKP2
EP300
E2F5
MDM2
CDKN1B (p27)
Downregulated 21 genes
Upregulated 4 genes
Vehicle
Lansoprazole
c
0 h
24 h
LPZ (-)
LPZ (-)
LPZ (+)
Cell Number (%)
PI Fluorescence
d
% of Cells
100
90
80
70
60
20
10
0
**
**
G0/G1
S
G2/M
LPZ - - + - + - +
Time 0h 12h 18h 24h
e
Vehicle LPZ
Skp2 (48 kDa)
βactin (45 kDa)
Relative expression 1.00 0.50
Vehicle LPZ
CDK2 (33 kDa)
βactin (45 kDa)
Relative expression 1.00 0.80
p27 (27 kDa)
βactin (45 kDa)
Relative expression 1.00 3.60
Cyclin E1 (48 kDa)
βactin (45 kDa)
Relative expression 1.00 0.65
f
Lansoprazole
Skp2
p27
p27
CDK2
Cyclin E
G1 arrest
Cell cycle